Published in final edited form as:
Nat Mater. ; 10(7): 545–552. doi:10.1038/nmat3049.

Nanoparticles that Communicate *In Vivo* to Amplify Tumour Targeting

Geoffrey von Maltzahn[1], **Ji-Ho Park**[2], **Kevin Y. Lin**[1], **Neetu Singh**[1], **Christian Schwöppe**[3], **Rolf Mesters**[3], **Wolfgang E. Berdel**[3], **Erkki Ruoslahti**[4,5], **Michael J. Sailor**[6], and **Sangeeta N. Bhatia**[1,7]

[1]Harvard-MIT Division of Health Sciences and Technology, Massachusetts Institute of Technology, 77 Massachusetts Avenue, Cambridge, MA 02139 (USA)

[2]Department of Bio and Brain Bioengineering; Korean Advanced Institute of Science and Technology; Chung Moon Soul Bldg (E-16) #1105; 291 Daehak-ro, Yuseong-gu, Dajeon, South Korea

[3]Department of Medicine/Hematology and Oncology, University Hospital Muenster, D-48129 Muenster, Germany

[4]Vascular Mapping Center, Burnham Institute for Medical Research at UCSB, Biology II Bldg., University of California, Santa Barbara, CA 93106-9610, (USA)

[5]Cancer Research Center, Burnham Institute for Medical Research, 10901 N. Torrey Pines Rd., La Jolla, CA 92037, (USA)

[6]Materials Science and Engineering Program, Department of Chemistry and Biochemistry, University of California, San Diego, 9500 Gilman, La Jolla, CA 92093 (USA)

[7]Electrical Engineering and Computer Science, MIT, David H. Koch Institute for Integrative Cancer Research, MIT, Department of Medicine, Brigham and Women's Hospital, Howard Hughes Medical Institute

Abstract

Nanomedicines have enormous potential to improve the precision of cancer therapy, yet our ability to efficiently home these materials to regions of disease *in vivo* remains very limited. Inspired by the ability for communication to improve targeting in biological systems, such inflammatory cell recruitment to sites of disease, we construct systems where synthetic biological and nanotechnological components communicate to amplify disease targeting *in vivo*. These systems are composed of 'Signalling' modules (nanoparticles or engineered proteins) that target tumours and then locally active the coagulation cascade to broadcast tumour location to clot-targeted 'Receiving' nanoparticles in circulation that carry a diagnostic or therapeutic cargo, thereby amplifying their delivery. We show that communicating nanoparticle systems can be composed from multiple types of Signalling and Receiving modules, can transmit information via multiple molecular pathways in coagulation, can operate autonomously, and can target over 40-fold higher doses of chemotherapeutics to tumours than non-communicating controls.

Advances in nanotechnology have produced a diverse toolkit of individual nanodevices with unique electromagnetic properties [1–3] and the ability to encapsulate and programmably

CORRESPONDENCE: For correspondence and requests for materials please contact Sangeeta N. Bhatia: sbhatia@mit.edu.

AUTHOR CONTRIBUTIONS:

GvM and SB conceived of the communication strategy, analyzed results, and wrote the manuscript; GvM, JP, KYL designed and performed experiments; CS, RM, WEB, ER, and MJS contributed reagents and technical expertise.

release a diversity of therapeutics,[4–9] yet the ultimate biomedical efficacy of such devices largely depends on their *in vivo* fate. Over the past three decades, approaches to targeting nanomaterials *in vivo* have focused on tuning the properties of individual nanoparticles including geometry, surface chemistry, ligand type and ligand density[10–18]. These materials are typically administered as populations of >1 trillion nanoparticles to carry out identical, competitive functions *in vivo*. Here, inspired by the power of communication to improve targeting across multiple length scales in biological systems (e.g. insect swarming, immune cell trafficking, platelet self-assembly), we considered the design of nanoparticle (NP) systems that communicate to enhance *in vivo* diagnostics, regenerative medicines, and therapeutics.

We set out to construct two-component nanosystems from well-characterized nanoparticle and biological components, wherein Signalling modules would first target tumours and then broadcast the tumour's location to Receiving nanoparticles in circulation (Figure 1A). To facilitate rapid and robust signal transmission in regions of tumour growth, we sought to harness the machinery of an endogenous multi-step biological cascade to transmit communications (Figure 1B) and selected the coagulation cascade due to its powerful signal amplification, positive feedback, ubiquitous presence in plasma, and potential to operate across multiple tumour types (Figure 1C). We hypothesized that two Signalling modules could selectively activate the coagulation cascade in tumours: nanoparticles (gold nanorods) that target tumours and convert external electromagnetic energy into heat in order to locally disrupt tumour vessels; and engineered human proteins (tumour-targeted tissue factor) that autonomously survey host vessels for angiongenic tumour receptors and, in their presence, activate the extrinsic coagulation pathway (Figure 1C). Receiving modules were constructed using two nanomaterial platforms: a prototypical imaging agent (magnetofluorescent iron oxide nanoworms) and a prototypical therapeutic agent (doxorubicin-loaded liposomes). We explored the potential to route communication to Receivers via two molecular pathways in coagulation by developing peptide coatings that recognize fibrin directly and peptides that target coagulation enzyme activity by acting as a substrate for the coagulation transglutaminase Factor XIII (FXIII) (**Scheme 1C).**

We first set out to examine the capacity of Signalling modules to precisely induce coagulation in tumours (Figure 2A). To test our hypothesis that photothermal heating of gold nanorods (NRs) could disrupt tumour blood vessels to initiate extravascular coagulation,[19–22] we examined the transduction of tumour heating into localized coagulation by evaluating fibrin deposition in tumours as a function of temperature (Figure 2A). Purified fibrinogen (the precursor to fibrin) and albumin (an abundant blood protein unrelated to coagulation) were labeled with unique near-infrared fluorochromes to allow simultaneous assessment of coagulation-dependent and independent protein tropism to heated tumours. Mixtures of fibrinogen and albumin were intravenously injected into athymic (*nu/nu*) mice bearing bilateral human MDA-MB-435 tumours, after which one tumour was heated using a temperature-controlled water bath. At 24 hours, mice were sacrificed and the relative levels of tumour fibrin(ogen) and albumin were assessed fluorescently. We observed a marked induction of fibrin(ogen) accumulation in tumours between 45oC and 53oC, with little accompanying increase in albumin accumulation, indicating that heat specifically directed coagulation cascade activation in tumours (Figure 2B, S1). Immunohistochemical staining for fibrin(ogen) in tumours from uninjected mice corroborated these findings, demonstrating that exogenous fibrinogen administration did not artificially drive accumulation in heated tumours (Figure S1).

Having probed the thermal sensitivity of coagulation in tumours, we next investigated whether tumour-targeted gold NRs could specifycoagulation to occur in tumour tissues. Rod-shaped gold nanoparticles are precisely-tunable plasmonic nanomaterials that may be

synthesized in bulk, have narrow size distributions, optical absorption coefficients 10^4–10^6-fold higher than conventional organic fluorochromes[19–21]. Previously, we demonstrated that polyethyleneglycol-coated gold NRs (PEG-NRs) have >17 hr circulation half-lives in mice and can passively target tumours in mice via their fenestrated angiogenic blood vessels to direct precise tumour heating with otherwise benign near-infrared (NIR) energy (Figure S2). [2324,25] Because near-infrared light can penetrate several cm's in human tissue, it provides an attractive external input to actuate vascular disruption in tumours[26]. To examine NR-directed coagulation, PEG-NRs (10 mg Au/kg) or saline were intravenously administered to mice bearing bilateral MDA-MB-435 tumours (Figure 2C, 2D). After PEG-NR clearance from circulation (72 hrs post-injection), fluorescent fibrinogen was intravenously injected and the right flanks of mice were irradiated with near-infrared light (~1 W/cm^2), generating focal tumour surface temperatures of ~49 C in PEG-NR-injected mice, while saline-injected tumour surface temperatures remained below ~37 C (Figure 2C). At 24 hrs post-injection, irradiated tumours on NR-injected mice displayed localized accumulation of fibrinogen (Figure 2D), while tumours with PEG-NRs or near-infrared energy alone and peripheral tissues lacked this feature. Histopathological analysis revealed that fibrin(ogen) deposition formed a broad interstitial mesh in heated tumours, indicating that NR heating could disrupt tumour blood vessels to activate extravascular coagulation (Figure S2).

We next investigated the potential for a biological Signalling module to autonomously survey the host vasculature for angiogenic tumour receptors and, in their presence, engage the extrinsic coagulation cascade. Such a system would operate without the need for any external electromangetic inputs (e.g. near-infrared energy) and could potentially amplify nanoparticle targeting to deep-seeded and disseminated cancers. We utilized a truncated, tumour-targeted version of the human protein tissue factor (tTF-RGD), which harnesses an RGD peptide motif to induce coagulation upon binding to angiogenic $\alpha_v\beta_3$ receptors[27–31] (Figure 2E). When tTF is separated from essential cell surface lipid co-factors, its activity towards Factor X activation diminishes by 5 orders of magnitude[32]. This nearly digital dependence on cell surface localization has enabled tumour-targeted tTFs to specifically activate coagulation in mouse cancer models and, recently, in human cancer patients[27,28]. As with PEG-NR Signalling modules, we first probed the relative accumulation of fluorescently-labeled fibrinogen and albumin in MDA-MB-435 tumours of mice injected with varying doses of tTF-RGD proteins. At 24 hours after injection, we observed a macroscopic appearance of hemorrhage in tumours on mice injected with tTF-RGD (>15 μg tTF-RGD/mouse), corresponding to the tumour-specific accumulation of fibrinogen in dendritic, vascular patterns, which were absent in control tumours (Figure 2F, 2G, S3). Microscopically, this appearance of vascular coagulation was corroborated by the abundant localization of fibrin(ogen) within tumour blood vessels (Figure 2G).

Together, we found that both PEG-NR and tTF-RGD Signalling modules produced tumour-specific coagulation, highlighting the potential for localized coagulation to communicate the tumour's location to Receivers in circulation. We next set out to develop Receiving nanoparticles that could efficiently target regions of coagulation to deliver therapeutics or act as imaging agents (Figure 3A). Initially, magnetofluorescent iron oxide nanoworm imaging agents (NWs) (Figure 3B top) were derivatized with a peptide substrate for the coagulation transglutaminase Factor XIII (G-N-***Q***-E-Q-V-S-P-L-T-L-L-K-X-C-Fluorescein)[33–35] to enable Receiver incorporation into regions of active coagulation (Figure 3B bottom, S4). Having observed that external heating of tumours produced localized coagulation, we utilized this response in an assay to assess the ability of Receivers to target tumour coagulation prior to integrating them with Signalling modules. Mixtures of targeted and untargeted NWs, labelled with unique near-infrared fluorochromes, were intravenously injected into mice bearing two MDA-MB-435 tumours. Immediately following injection,

one tumour was submerged in a temperature-controlled water bath for 20 min and mice were dissected at 24 hrs for fluorescent organ imaging. We found that the accumulation of FXIII-NW Receivers was sharply amplified at 45oC compared to FXIIIControl-NWs bearing peptides without the essential glutamine for FXIII cross-linking (Figure 3C, 3D, S5), enabling nearly an order of magnitude increase in tumour targeting compared to unheated tumours. The specificity of heat-induced targeting to coagulation persisted up to 53oC, although the magnitude of accumulation decreased (Figure 3E), likely indicating that higher temperatures accelerated intravascular coagulation and occlusion, diminishing the perfusion required for delivery of Receiving NWs into tumours. Histopathologically, FXIII- NWs showed marked extravasation and interstitial spreading in heated tumours compared with controls (Figure 3D, S5), illustrating the capacity of thermal energy to dismantle tumour vascular barriers and direct abundant interstitial Receiver accumulation.

We also explored the feasibility of channelling communications via an alternative molecular pathway in the coagulation cascade. NWs were derivatized with a fibrin-binding peptide (Ac-d-d-d-***G-Y-e-C-hyP-cY-G-L-C-Y-I-Q***-K-Fluorescein) (Figure 3B) and tested in a similar assay. Fibrin-binding Receiving NWs also exhibited nearly a 10-fold amplification of targeting to heated tumours (Figure 3C, S5), with prominent extravascular accumulation histopathologically (Figure S5).

We next constructed model therapeutic Receiving modules to provide amplified drug delivery to regions of tumour coagulation. Therapeutic Receivers were developed by synthesizing doxorubicin-loaded liposomes (LPs) with tethered active (FXIII) or inactive (FXIIIControl) substrates (Figure S4, S6). Here, tumour heating to 45oC directed the accumulation of over 40-times higher doses of doxorubicin in tumours compared with unheated controls and significantly enhanced targeting over inactive FXIIIControl substrate-modified LPs (Figure 3F).

Having developed Signalling and Receiving modules and characterized their function in isolation, we proceeded to study the ability of integrated nanoparticle systems to communicate and amplify tumour targeting *in vivo* (Figure 4A). We began by testing the ability for communication to amplify the targeting of magnetofluorescent FXIII-NW Receiving modules to tumours. PEG-NRs (or saline) were intravenously-injected into mice bearing bilateral MDA-MB-435 tumours. After NR clearance from circulation (72 hrs), mixtures of active and inactive Receiving nanoparticles (FXIII-NWs and FXIIIControl-NWs) labelled with distinct near-infrared fluorochromes were co-injected intravenously, followed by near-infrared irradiation of the entire right flank of the mouse (~0.75 W/cm^2, 810 nm, 20 min) under infrared thermographic observation. At 96 hrs, the entire mouse and then the individual explanted organs were fluorescently imaged (Figure 4B). Thermographic surveillance of photothermal heating showed focal tumour heating only in NR-injected mice (Figure 4C) and whole-animal imaging at 96 hrs revealed pronounced homing of FXIII-NWs to NR-heated tumours, with over an order of magnitude increase in accumulation above unirradiated contralateral tumours and tumours on saline-injected mice (Figure 4D, 4E, S7). Histologically, integrated nanoparticle systems produced intense regions of FXIII-NW fluorescence relative to controls, particularly in tumour boundaries where blood vessels were well perfused (Figure S8). Nanoparticle systems were found to be effective in xenograft cervical tumour models as well, directing several fold amplification in homing of targeted Receiving nanoparticles over untargeted controls (Figure S9).

We next probed the ability for autonomous communication between tTF-RGD Signalling modules and FXIII-NW Receiving modules to amplify tumour targeting (Figure 4F). When co-injected alongside FXIII-NW Receivers (Figure 4G), we find that tTF-RGD Signalling modules amplify Receiver targeting by several fold over non-communicating controls and

over NWs that are directly targeted by RGD-targeting ligands (Figure 4H, S10). Similar to the fibrin(ogen) distribution observed during tTF-RGD Signalling module testing, FXIII-NW Receivers injected alongside tTF-RGD proteins produced a dendritic pattern of accumulation in tumours, corresponding to abundant intravascular localization immunohistochemically (Figure 4H, 4I, 4J). This amplified vascular targeting was found to be specific for tumours over normal organs and was absent when the coagulation-inhibitor heparin was administered alongside Signalling and Receiving modules (Figure 4I, S10). Further, we found that tTF-NGR Signalling modules, which target CD13 angiogenic receptors, were also able to amplify Receiver targeting to tumours (Figure S10), highlighting the capacity for autonomously-communicating systems to be customized for specific molecular cancer signatures.

As a proof of principle that nanoparticle communication could improve tumour drug delivery and therapy, we studied the efficacy of a therapeutic communicating nanosystem (Figure 5A). We found that communication between NR Signalling modules and FXIII-LP Receivers amplified the accumulation of doxorubicin in tumours by over 40-fold (~8% ID/g) as compared to the LPs alone (Figure 5B) and >6-fold when compared to an optimized liposome formulation that targeted endogenous vascular receptors ($\alpha_v\beta_3$ for high affinity cyclic-RGD peptide-targeted LPs), illustrating the potential for nanoparticle communication to amplify drug delivery over nanoparticles directly targeted to tumour receptors (Figure S11). This amplification of drug delivery likely has at least two components: heat-dependent increases in passive accumulation due to improved extravasation in tumours (as indicated by FXIIIControl-LPs and consistent with previous observations[22]) and specific biochemical recognition of the coagulation process by the peptide coating. Histologically, FXIII-LPs formed a broad interstitial mesh in NR-heated tumours, with released doxorubicin fluorescence emanating from the nuclei of surrounded tumour cells, confirming the delivery and release of active drug within tumour tissues (Figure 5C).

We finally evaluated the therapeutic efficacy of communicating nanoparticles in mice bearing single MDA-MB-435 human carcinoma tumours. PEG-NRs (10 mg/kg) or saline were injected into mice and, once NRs had cleared from circulation (72 hrs), a single intravenous dose of FXIII- LPs, FXIIIControl -LPs, or saline (2 mg/kg doxorubicin) was given, followed immediately by irradiation with near-infrared energy (~0.75 W/cm^2, 810 nm, 20 min). We found that a single treatment with communicating nanoparticles directed a prolonged inhibition of tumour growth that was significantly more effective than system components in isolation (FXIII-LPs, FXIIIControl-LPs, NRs) and non-communicating control systems (NRs + FXIIIControl-LPs) (Figure 5D, 5E) ($p<0.02$ for NR + FXIII-LPs compared to all other treatment groups at each day from 5–24 after treatment; one-sided t-test) without detectable weight loss due to systemic toxicity (Figure S11).

Inspired by communication in biological systems, we devised the first nanoparticle systems that communicate to amplify tumour targeting. We demonstrate that systems of synthetic human proteins and simple nanoparticles can be engineered to transmit information through endogenous biological pathways by acting as artificial inputs and outputs to the coagulation cascade. In contrast with ‘combination’ therapies where multiple disease pathways in the host are targeted simultaneously, our strategy is composed of components that communicate with one another to more efficiently target regions of disease. We found that communication via the coagulation cascade enhanced the accumulation of Receiving modules in tumours by up to 40-fold relative to Receiving modules tested in the absence of communication (Figure S12), Further, we found that, after subtracting the baseline targeting of Receivers without communication, each NR Signalling module in a host tumour was able to recruit >150 FXIII- NWs or >35,000 doxorubicin molecules encapsulated within FXIII- LPs (Figure S12), demonstrating the capacity for signal amplification in our approach. Similarly, each

tTF-RGD Signalling module that accumulated in a host tumour was able to recruit >10 FXIII- NWs via induction of localized coagulation (Figure S12). The ability for each tumour receptor-targeted tTF-RGD Signalling module in our system to recruit many nanoparticle Receiving modules contrasts to conventional strategies for ligand-mediated nanoparticle targeting where, depending on nanoparticle valency, one or fewer nanoparticles are delivered per ligand-bound receptor in tumours.

We believe this work motivates a new paradigm of 'systems nanotechnology' directed toward the construction of communicative diagnostic and therapeutic agents with sophisticated *in vivo* behaviours. Given the diverse nanoparticle and synthetic biological 'building blocks' under development[13–18,36–38], coupled with the plethora of robust biological cascades that could be re-purposed to enable communication between synthetic components, we believe that a wide array of nanosystems could be engineered to more sensitively locate, diagnose, and treat a diversity of focal human diseases.

Materials and Methods (detailed methods provided in Supplemental Materials)

Signalling Module Synthesis

Long-circulating *PEG-NRs* were synthesized with 5kDa mPEG-thiol coatings as described previously(23) and tTF-RGD and tTF-NGR Signalling modules were expressed in engineered *Escherichia coli*, purified, and tested in vitro to verify purity (>95%) and activity (Factor-X coagulation test) as described in Supplemental Materials.

Receiving Module Synthesis

Peptide Synthesis—The three peptides used in this work were synthesized via FMOC solid-phase peptide synthesis, HPLC-purified to >90% purity, and characterized via mass spectrometry as described in Supplemental Materials.

Iron oxide NW synthesis—Superparamagnetic, dextran-caged iron oxide nanoworms (NWs) with a longitudinal size of ~55 nm were synthesized, aminated using 20% v/v ammonium hydroxide, and derivatized with near-infrared fluorophores as described previously(11). All peptide-functionalized NWs were characterized via dynamic light scattering (DLS) and intravenously injected *in vivo* to ensure all targeted NWs and control NWs exhibited similar circulation times. NIR-fluorophore and peptide attachment protocols, along with NW purification methods, provided in Supplemental Materials.

Doxorubicin-loaded liposome synthesis—Hydrogenated soy sn-glycero-3-phosphocholine (HSPC), cholesterol, and 1,2-distearoyl-snglycero-3-phosphoethanolamine-N-polyethylene glycol 2000 [DSPE-PEG(2k)], 1,2-Distearoyl-sn-Glycero-3-Phosphoethanolamine-N-[Maleimide(Polyethylene Glycol 2000)] [DSPE-PEG(2k)-MAL] were purchased from Avanti Polar Lipids (Alabaster, AL). Doxorubicin was purchased from Sigma Chemical Co. (St.Louis, MO). Briefly, for targeted LP synthesis, liposomes with maleimide groups were prepared from HSPC, cholesterol, DSPE-PEG(2k), and DSPE-PEG(2k)-MAL by lipid film hydration and membrane extrusion. Encapsulation of doxorubicin (DOX) into the liposomes was then carried out using a pH gradient-driven loading protocol. Free doxorubicin was removed by gel filtration on Sephadex G-50 and the maleimide-terminated liposomes were reacted with thiols on peptides (FXIII and FXIIIControl) for 2 hrs and then purified by gel filtration.

In Vivo Studies

All studies in mice were approved by the Massachusetts Institute of Technology Committee on Animal Care. MDA-MB-435 human cancer cells were cultured as recommended by ATCC and injected into nu/nu mice to establish xenograft tumours as described previously (3, 11, 23).

Signalling module distribution and bioactivity in vivo—Signalling module biodistribution and fibrinogen coagulation assays are provided in Supplemental Materials.

Immunohistochemical analysis in tumours—For histologic analysis, frozen sections of tumours were prepared. The sections were first fixed with acetone. Rat anti-mouse CD-31 (1:50, BD PharMingen) and biotinylated mouse fibrin(ogen) antiserum (1:50, Nordic) were used for immunochemical staining of tumour tissue sections. The corresponding secondary antibodies were added and incubated for 1 hour at room temperature: AlexaFluor-594 goat anti-rat or rabbit IgG (1:1,000; Molecular Probes), streptavidin Alexa Fluor 594 (1:1000; Molecular Probes). The slides were washed three times with PBS and mounted in Vectashield Mounting Medium with DAPI. At least three images from representative microscopic fields were analyzed for each tumour sample.

Imaging Receiving NW homing to tumours—Mixtures of NIR-fluorophore-labelled, targeted and control NWs (bearing VT750 and VT680 or VT680 and VT750, respectively) were co-adminstered intravenously in PBS (2 mg Fe/kg) to tumour-bearing nu/nu mice to provide an internal control reference for coagulation-specific NW homing. At 24 hrs post-NW injection, mice were sacrificed and organs were analyzed for both NIR-fluorophores (LI-COR Odyssey Infrared Imaging System). For integrated nanoparticle system characterization, mice were additionally imaged under isofluorane anaesthetic before euthanization using a whole animal fluorescence reflectance imaging system (Xenogen, IVIS Imaging System) to visualize the specificity of NW homing to tumours. Images from both organ scanning and whole animal imaging are displayed throughout the manuscript as overlaid green/red images from both fluorescence channels (VT750=green and VT680=red). For autonomously-communicating nanosystems, NIR-fluorophore-labeled peptide-bearing NWs (bearing VT750 fluorophores) were intravenously (2 mg Fe/kg) in PBS to unanaesthetized MDA-MB-435 tumour-bearing nu/nu mice alone or alongside various tTF Signalling modules (25 μg). At 24 hrs post-NW injection, mice were sacrificed and organs were analyzed for NIR Receiver fluorescence (LI-COR Odyssey Infrared Imaging System). For intraoperative fluorescent tumour imaging, mice were anaesthesized and tumours were surgically exposed to reveal detailed tumour fluorescence (LI-COR). For whole animal organ distribution, tTF-RGD Signalling modules were administered intraperitoneally (25 μg) and FXIII-NWs were administered intravenously (2 mg Fe/kg) to mice bearing a single MDA-MB-435 tumour.

Quantification of Receiver homing to tumours—Protocols for fluorescent quantification of NW and doxorubicin quantification provided in Supplemental Materials.

Therapeutic assessment of communicating and control nanoparticle systems—Therapeutic studies were conducted by first intravenously administering PEG-NRs or saline into nu/nu mice bearing a single MDA-MB-435 tumour. At 72 hrs post-injection, mice were intravenously administered FXIII- LPs, FXIIIControl- LPs, or saline (in ~150 μl bolus) and broadly irradiated in the vicinity of the tumour with NIR light (810 nm, ~1 W/cm^2, 20 min). An additional cohort of mice was administered saline at 0 and 72 hrs and not exposed to NIR light in order to isolate any therapeutic efficacy of this input in isolation. At

regular intervals after treatment, tumours were measured and mice were weighed. Mice were sacrificed when tumours exceeded 500 mm^3.

Supplementary Material

Refer to Web version on PubMed Central for supplementary material.

Acknowledgments

This work was supported by the National Cancer Institute of the National Institutes of Health through grant numbers U54 CA 119335 (UCSD CCNE), 5-R01-CA122427 (Bioengineering Research Partnerships, BRP), and U54 CA119349 (MIT CCNE). The authors thank Peter Caravan for assistance with the fibrin-binding peptide selection and testing; Daniel Kim, Steven Mo, Luvena Ong, and Mary Xu for assistance with *in vivo* studies; and Ralph Weissleder for assistance with preliminary fluorescent imaging studies.

References

1. Chan WC, Nie S. Quantum dot bioconjugates for ultrasensitive nonisotopic detection. Science. 1998; 281:2016–2018. [PubMed: 9748158]
2. Park JH, et al. Magnetic iron oxide nanoworms for tumour targeting and imaging. Advanced Materials. 2008; 20:1630. [PubMed: 21687830]
3. Xia YN, Halas NJ. Shape-controlled synthesis and surface plasmonic properties of metallic nanostructures. Mrs Bulletin. 2005; 30:338–344.
4. Gref R, et al. Biodegradable long-circulating polymeric nanospheres. Science. 1994; 263:1600–1603. [PubMed: 8128245]
5. Sengupta S, et al. Temporal targeting of tumour cells and neovasculature with a nanoscale delivery system. Nature. 2005; 436:568–572. [PubMed: 16049491]
6. Park JH, von Maltzahn G, Ruoslahti E, Bhatia SN, Sailor MJ. Micellar hybrid nanoparticles for simultaneous magnetofluorescent imaging and drug delivery. Angewandte Chemie-International Edition. 2008; 47:7284–7288.
7. Litzinger DC, Huang L. Phosphatidylethanolamine Liposomes - Drug Delivery, Gene-Transfer and Immunodiagnostic Applications. Biochimica Et Biophysica Acta. 1992; 1113:201–227. [PubMed: 1510997]
8. Akinc A, et al. A combinatorial library of lipid-like materials for delivery of RNAi therapeutics. Nature Biotechnology. 2008; 26:561–569.
9. Anderson DG, Lynn DM, Langer R. Semi-automated synthesis and screening of a large library of degradable cationic polymers for gene delivery. Angewandte Chemie-International Edition. 2003; 42:3153–3158.
10. Leserman LD, Barbet J, Kourilsky F, Weinstein JN. Targeting to cells of fluorescent liposomes covalently coupled with monoclonal antibody or protein A. Nature. 1980; 288:602–604. [PubMed: 7442804]
11. Heath TD, Fraley RT, Papahdjopoulos D. Antibody targeting of liposomes: cell specificity obtained by conjugation of F(ab′)2 to vesicle surface. Science. 1980; 210:539–541. [PubMed: 7423203]
12. Akerman ME, Chan WCW, Laakkonen P, Bhatia SN, Ruoslahti E. Nanocrystal targeting in vivo. Proceedings of the National Academy of Sciences of the United States of America. 2002; 99:12617–12621. [PubMed: 12235356]
13. Hood JD, et al. Tumour regression by targeted gene delivery to the neovasculature. Science. 2002; 296:2404–2407. [PubMed: 12089446]
14. Farokhzad OC, et al. Nanoparticle-aptamer bioconjugates: A new approach for targeting prostate cancer cells. Cancer Research. 2004; 64:7668–7672. [PubMed: 15520166]
15. Weissleder R, Kelly K, Sun EY, Shtatland T, Josephson L. Cell-specific targeting of nanoparticles by multivalent attachment of small molecules. Nature Biotechnology. 2005; 23:1418–1423.
16. Geng Y, et al. Shape effects of filaments versus spherical particles in flow and drug delivery. Nature Nanotechnology. 2007; 2:249–255.

17. Moghimi SM, Hunter AC, Murray JC. Long-circulating and target-specific nanoparticles: Theory to practice. Pharmacological Reviews. 2001; 53:283–318. [PubMed: 11356986]
18. Moghimi SM, Szebeni J. Stealth liposomes and long circulating nanoparticles: critical issues in pharmacokinetics, opsonization and protein-binding properties. Progress in Lipid Research. 2003; 42:463–478. [PubMed: 14559067]
19. Murphy CJ, et al. Anisotropic metal nanoparticles: Synthesis, assembly, and optical applications. J Phys Chem B. 2005; 109:13857–13870. [PubMed: 16852739]
20. Jain PK, Lee KS, El-Sayed IH, El-Sayed MA. Calculated absorption and scattering properties of gold nanoparticles of different size, shape, and composition: Applications in biological imaging and biomedicine. J Phys Chem B. 2006; 110:7238–7248. [PubMed: 16599493]
21. Hu M, et al. Gold nanostructures: engineering their plasmonic properties for biomedical applications. Chem Soc Rev. 2006; 35:1084–1094. [PubMed: 17057837]
22. Kong G, Braun RD, Dewhirst MW. Hyperthermia enables tumour-specific nanoparticle delivery: Effect of particle size. Cancer Research. 2000; 60:4440–4445. [PubMed: 10969790]
23. von Maltzahn G, et al. Computationally-guided photothermal tumour therapy using long-circulating gold nanorod antennas. Cancer Research. 2009; 69 (9):3892. [PubMed: 19366797]
24. Hashizume H, et al. Openings between defective endothelial cells explain tumour vessel leakiness. Am J Pathol. 2000; 156:1363–1380. [PubMed: 10751361]
25. Maeda H. The enhanced permeability and retention (EPR) effect in tumour vasculature: the key role of tumour-selective macromolecular drug targeting. Adv Enzyme Regul. 2001; 41:189–207. [PubMed: 11384745]
26. Weissleder R. A clearer vision for in vivo imaging. Nature Biotechnology. 2001; 19:316–317.
27. Kessler T, et al. Inhibition of tumour growth by RGD peptide-directed delivery of truncated tissue factor to the tumour vasculature. Clinical Cancer Research. 2005; 11:6317–6324. [PubMed: 16144936]
28. Bieker RKT, Schwoppe C, Padro T, Persigehl T, Bremer C, Dreischaluck J, Kolkmeyer A, Heindel W, Mesters RM, Berdel WE. Infarction of tumour vessels by NGR-peptide directed targeting of tissue factor. Experimental results and first-in-man experience. Blood. 2009 In Press.
29. Huang XM, et al. Tumour infarction in mice by antibody-directed targeting of tissue factor to tumour vasculature. Science. 1997; 275:547–550. [PubMed: 8999802]
30. El-Sheikh A, Borgstrom P, Bhattacharjee G, Belting M, Edgington TS. A selective tumour microvasculature thrombogen that targets a novel receptor complex in the tumour angiogenic microenvironment. Cancer Research. 2005; 65:11109–11117. [PubMed: 16322261]
31. Persigehl T, et al. Antiangiogenic tumour treatment: Early noninvasive monitoring with USPIO-enhanced MR imaging in mice. Radiology. 2007; 244:449–456. [PubMed: 17562810]
32. Paborsky LR, Caras IW, Fisher KL, Gorman CM. Lipid association, but not the transmembrane domain, is required for tissue factor activity. Substitution of the transmembrane domain with a phosphatidylinositol anchor. J Biol Chem. 1991; 266:21911–21916. [PubMed: 1834663]
33. Jaffer FA, et al. Molecular imaging of factor XIIIa activity in thrombosis using a novel, near-infrared fluorescent contrast agent that covalently links to thrombi. Circulation. 2004; 110:170–176. [PubMed: 15210587]
34. Tung CH, et al. Novel factor XIII probes for blood coagulation imaging. Chembiochem. 2003; 4:897–899. [PubMed: 12964167]
35. Overoye-Chan K, et al. EP-2104R: A fibrin-specific gadolinium-based MRI contrast agent for detection of thrombus. Journal of the American Chemical Society. 2008; 130:6025–6039. [PubMed: 18393503]
36. Isaacs FJ, Dwyer DJ, Collins JJ. RNA synthetic biology. Nature Biotechnology. 2006; 24:545–554.
37. Hasty J, McMillen D, Collins JJ. Engineered gene circuits. Nature. 2002; 420:224–230. [PubMed: 12432407]
38. Jungmann R, Renner S, Simmel FC. From DNA nanotechnology to synthetic biology. HFSP J. 2008; 2:99–109. [PubMed: 19404476]

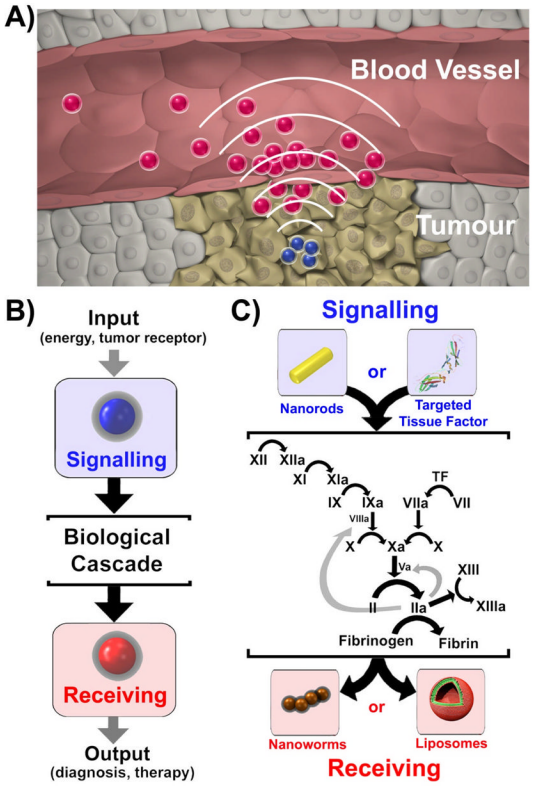

Figure 1. Nanoparticle communication for amplified tumour targeting

A) *Schematic representation of communication between system components*. Tumour-targeted Signalling nanoparticles broadcast tumour location to Receiving nanoparticles in circulation. **B)** *Harnessing a biological cascade to transmit and amplify nanoparticle communications.* **C)** *Molecular signalling pathway between Signalling and Receiving components.* Signalling and Receiving components act as unnatural inputs and outputs to the coagulation cascade, respectively. Signalling components are either tumour-targeted plasmonic gold nanorods (NRs), which initiate coagulation cascade activation in tumours by photothermally disrupting tumour vessels and activating the extrinsic and intrinsic coagulation pathways, or tumour-targeted truncated tissue factor proteins, which are latent in circulation and activate the extrinsic coagulation pathway upon binding to tumour receptors. Communication is exploited to recruit inorganic (iron oxide nanoworms) or organic (drug-loaded liposomes) Receiving components via activity of the coagulation transglutaminase FXIII or via targeting of polymerized fibrin.

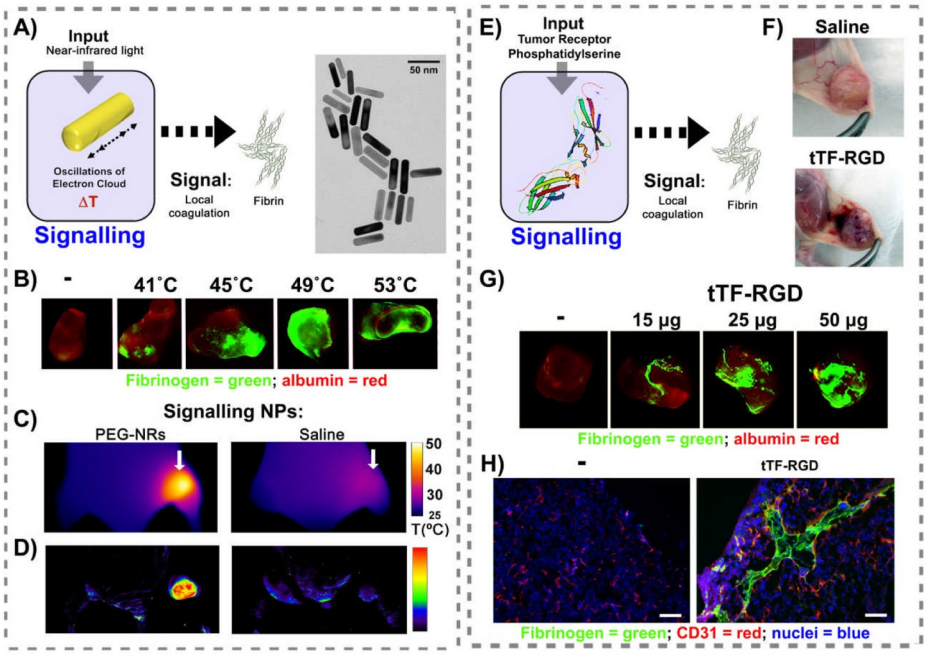

Figure 2. 'Signalling' component characterization

A) *Schematic of nanorod-directed coagulation and transmission electron microscopy of near-infrared absorbing nanorods.* Gold nanorods (NRs) are targeted to tumours to specify local coagulation cascade activation via photothermal conversion of near-infrared energy. **B)** *Probing the coagulation-dependent and -independent protein tropism to heated tumours.* Fibrinogen and albumin were labelled with unique near-infrared fluorochromes and injected into mice bearing bi-lateral MDA-MB-435 tumours. Immediately following injection, one tumour on each mouse was heated using a temperature-controlled water bath. At 24 hrs post-injection, mice were dissected and tumours imaged for the relative abundance of fibrinogen (green) and albumin (red). **C)**. *Thermographic imaging of PEG-NR- and saline-injected mice under near-infrared irradiation of the right flank.* **D)** *Fluorescence reflectance imaging of mice to visualize fibrinogen tropism to PEG-NR-heated tumours.* **E)** *Schematic of tumour-targeted tissue factor stimulation of the coagulation cascade in response to tumour receptors.* Signalling components are ligand-targeted, truncated human tissue factor proteins (tTF-RGD) proteins that are latent in circulation and autonomously gain coagulation-inducing activity upon binding to $\alpha_v\beta_3$ receptors in tumour blood vessels and associating with endothelial cell surface phosphatidylserine. **F)** *Intraoperative images at 24-hrs post-tissue factor injection revealing tTF-RGD-mediated haemorrhaging.* **G)** *Probing the coagulation-dependent and -independent protein tropism to tumours on tTF-RGD-injected mice*. tTF-RGD Signalling components were injected intravenously at varying doses alongside mixtures of fluorescent fibrinogen (green, VT750) and albumin (red, VT680) to monitor tTF-RGD-mediated coagulation in tumours. **H)** *Histopathologic analysis of tumour fibrinogen distribution without (left) and with 25µg tTF-RGD Signalling component co-injection (right)* (Red = CD31 blood vessel stain; Green = injected fibrinogen fluorescence; Blue = nuclear stain; scale bars=100 µm)

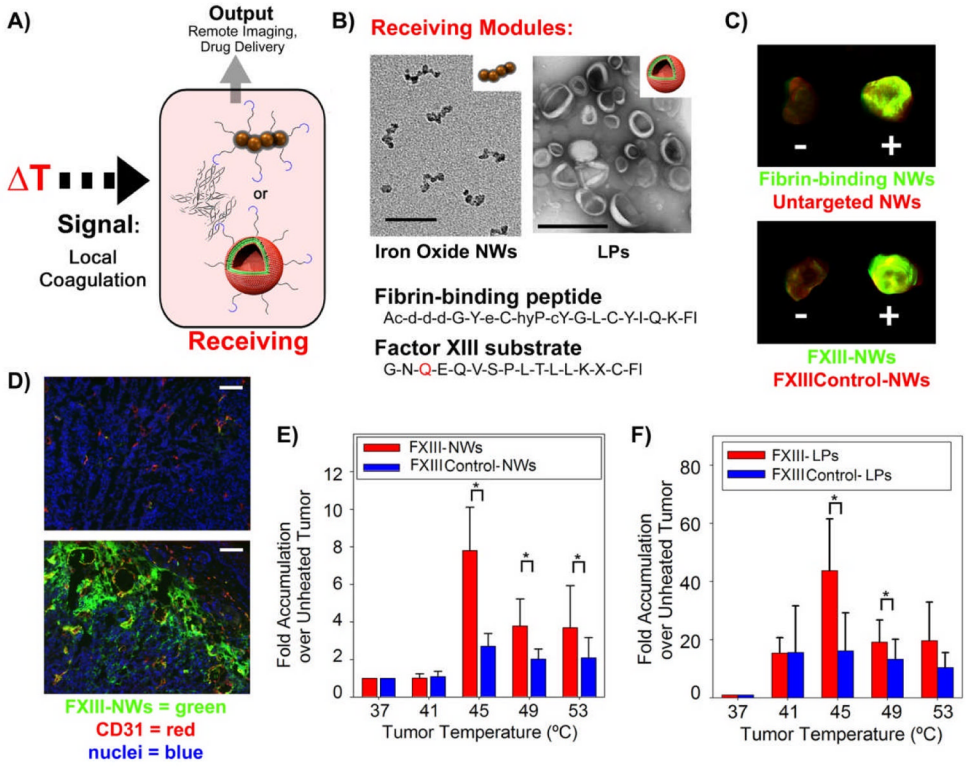

Figure 3. 'Receiving' component synthesis and testing

A) *Schematic of Receiving NP homing to regions of coagulation.* Nanoworm (NW) imaging agents and drug-loaded liposomes (LPs) (top and bottom, respectively) were derivatized with coagulation-targeting peptides to form Receiving NPs. **B)** *Nanostructure and targeting ligands of Receiving NPs.* Transmission electron microscopy images of the two classes of nanomaterials utilized in Receiving NP synthesis: iron oxide nanoworms (NWs; scale bar=50 nm) and doxorubicin-loaded liposomes (LPs; scale bar=400 nm). Two peptides were utilized to generate Receiving NPs: a fibrin-binding peptide and a glutamine-containing substrate for the coagulation transglutaminase FXIII to respectively direct particle binding and covalent attachment in regions of coagulation. **C)** *Fluorescence reflectance imaging of Receiving NP homing to externally-heated tumours.* Mixtures of targeted (green) and untargeted (red) NWs, labelled with the unique NIR-fluorochromes VT750 and VT680, respectively, were intravenously injected into mice bearing bilateral MDA-MB-435 tumours. Immediately following injection, one tumour was submerged in a temperature-controlled water bath for 20 min and mice were dissected at 24 hrs for fluorescent organ imaging. Overlaid fluorescence images are shown for targeted (green) and untargeted (red) Receiving NP accumulation in both heated (+, 45oC heating) and naïve (−) tumours from the same mouse. **D)** *Histopathological analysis of Receiving NP homing to heated tumours.* Histological sections from naïve (top) and heated (bottom, 45oC) tumours in FXIII-NW-injected mice were stained for CD31 (red) and nuclei (blue) and imaged to reveal Receiving NP distribution (green). (Scale bars = 100 μm) **E)** *Quantifying the amplification of FXIII-NW and FXIIIControl-NW Receiver homing to heated over unheated tumours.* The fold enhancement of NW targeting is plotted across the range of temperatures tested (p=0.02 and 0.03 for the difference between FXIII- -NWs and *FXIIIControl*-NWs at 45oC and 49oC, respectively; paired, two-sided t-test, n=4; error bars=std. dev.). **F)** *Quantifying the amplification of FXIII-LP and FXIIIControl–LP (Drug-loaded Liposome) Receiver homing to heated over unheated tumours.* The fold enhancement of doxorubicin accumulation in

tumours is plotted across the range of temperatures tested for FXIII- LPs and *FXIIIControl* -LPs ($p=0.025$ and $p=0.049$ for the difference between FXIII- NWs and *FXIIIControl*-NWs at 45oC and 49oC, respectively; unpaired, two-sided t-test, n=3; error bars=std. dev.).

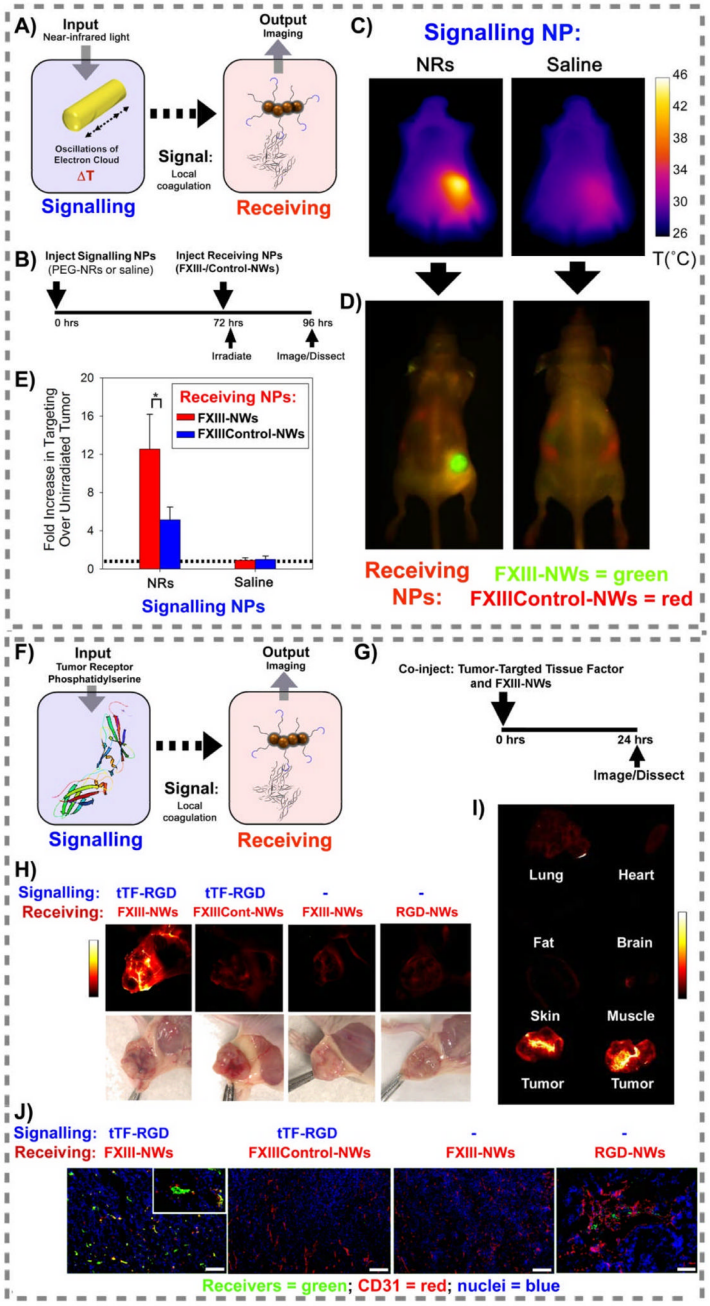

Figure 4. Amplified tumour targeting with two systems of communicating nanoparticles

A) *Schematic of communicating nanoparticles.* **B)** *Experimental timeline for testing communicating nanoparticles.* **C)** *Thermographic imaging of photothermal PEG-nanorod heating.* At 72 hrs post NR- or saline-injection (10 mg Au/kg), mice were co-injected with coagulation-targeted (FXIII- NWs) and untargeted (FXIIIControl-NWs) and their right flanks were broadly irradiated (810 nm, ~0.75 W/cm^2, 20 min) under infrared thermographic surveillance to reveal surface temperatures. **D)** *Overlaid fluorescence reflectance image of targeted and untargeted Receiving NP homing.* At 24 hrs post-irradiation, whole-animal fluorescence imaging revealed the distributions of coagulation targeted (FXIII-NWs, green) and untargeted (FXIIIControl-NWs, red) Receiving NPs. **E)** *Quantification of Receiving NP*

homing in irradiated vs contralateral unirradiated tumours. After whole-animal imaging, mice were dissected and the fluorescence of each tumour was measured to quantify the homing of Receiving NPs. (* indicates p=0.02, paired, two-sided t-test; n=4; error bars=std. dev.) **F)** *Schematic of a nanosystem that communicates autonomously in the presence of tumour receptors.* **G)** *Experimental timeline for testing the autonomous nanosystem in vivo.* **H)** *Intraoperative imaging of NW Receivers. Nu/nu* mice bearing a single MDA-MB-435 tumour were intravenously injected with communicating (tTF-RGD + FXIII-NWs) or control (tTF-RGD + FXIIIControl-NWs) systems, FXIII-NWs alone, or NWs targeted by the peptide used to direct Signalling component tumour homing (1 mg/kg tTF-RGD). At 24 hrs post-injection, tumours were surgically exposed for fluorescent intraoperative imaging of NW homing. (FXIIICont-NWs = FXIIIControl-NWs) **I)** *Tumour specificity of the autonomous nanosystem*. Excised organs from mice injected with autonomously communicating nanosystems (tTF-RGD + FXIII-NWs) were imaged for NW fluorescence at 24 hrs post-injection (1 mg/kg tTF-RGD). J) *Histopathological analysis of NW Receivers.* Histopathological sections from experiments in H). At 24 hrs post-NW injection, mice were sacrificed and tumours were analyzed for NW Receiver distribution in histology. (Red= CD31 blood vessel stain, Blue= DAPI nuclear stain, Green=NW Receiver distribution, RGD-NW scale bar=100 μm; All others = 200 μm)

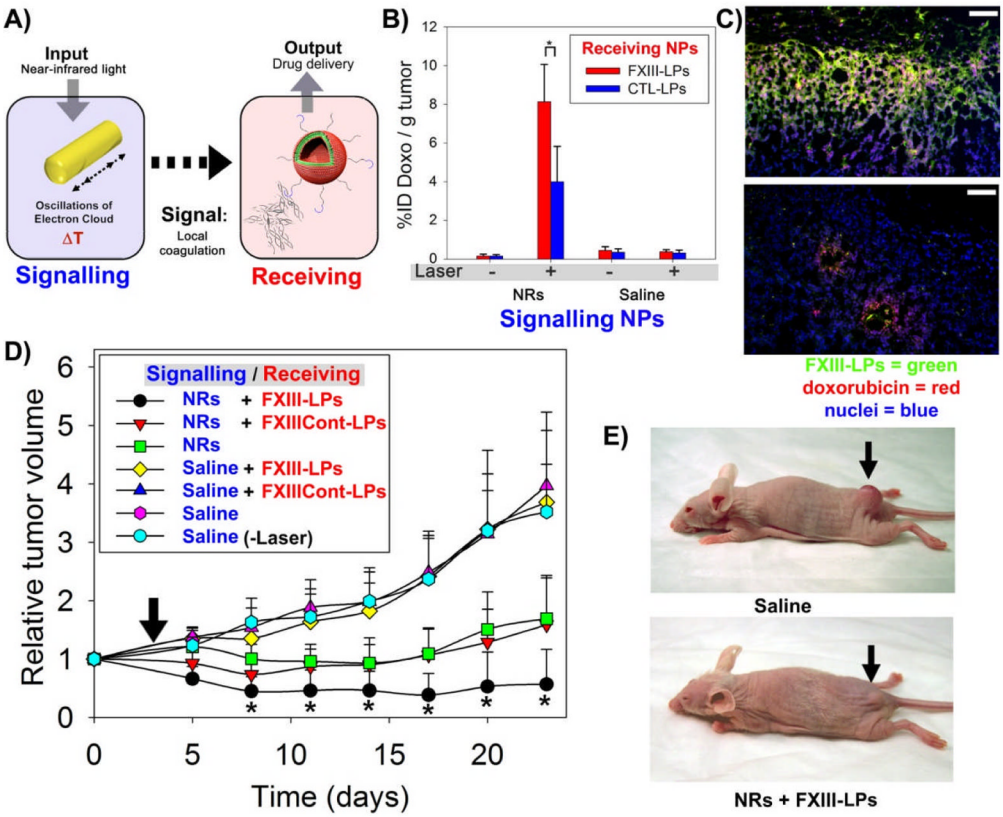

Figure 5. Amplified tumour therapy with communicating nanoparticles

A) *Schematic of therapeutic system of communicating nanoparticles* **B)** *Quantification of doxorubicin-loaded LP Receiver homing in irradiated vs contralateral unirradiated tumours.* At 96 hrs after Signalling NP injection, mice were dissected and the doxorubicin fluorescence of each tumour homogenate in acidic ethanol was measured to quantify the homing of Receiving NPs. (* indicates p=0.021, unpaired, two-sided t-test, n=4; error bars=std. dev.) **C)** *Histopathological analysis of NR-directed FXIII- LP targeting and doxorubicin delivery.* Histopathological sections from the integrated NP signalling experiments in B). At 24 hrs post-NW injection, mice were sacrificed and tumours were analyzed for FXIII-LP and doxorubicin distributions in histology. (Red= doxorubicin, Blue= DAPI nuclear stain, Green=FXIII- LP distribution). (Scale bars = 100 μm). **D)** *Tumour volumes following a single treatment with communicating nanoparticle systems and controls.* Tumours in all treatment groups except Saline (laser) were exposed to near-infrared irradiation for 20 min (~0.75 W/cm^2, ~810 nm, arrow) 72 hrs after i.v. nanorod or saline injection ($p<0.05$ for NR + FXIII-LPs and all other treatment sets between days 8 and 24; ANOVA, n=7 mice in each set). **E)** *Representative images of mice treated with communicating nanoparticles (NRs + FXIII-LPs, below) compared with untreated controls (Saline, above) (20 days post-treatment).*